Lasers in Surgery and Medicine 21:166–178 (1997)

Propagation of Fluorescent Light

A.J. Welch, PhD,* Craig Gardner, PhD, Rebecca Richards-Kortum, PhD, Eric Chan, MS, Glen Criswell, BS, Josh Pfefer, MS, and Steve Warren, PhD

Biomedical Engineering Program, University of Texas, Austin, Texas 78712

Background and Objective: **In general, the remitted fluorescence spectrum is affected by the scattering and absorption properties of tissue. Other important factors are boundary conditions, geometry of the tissue sample, and the quantum yield of tissue fluorophores. Each of these factors is examined through a series of Monte Carlo simulations.**
Study Design/Materials and Methods: **Monte Carlo modeling is used to simulate the propagation of excitation light and the resulting fluorescence. Remitted fluorescence is determined for semi-infinite single and multiple layer geometries and for cubic geometries representing small tissue samples. Monte Carlo results are compared to approximations obtained with a heuristic model.**
Results: **Remitted fluorescence as a function of (1) the depth of fluorescence generation and (2) radial escape position is presented for semi-infinite single and multiple layer geometries. Fluorescence from a small tissue sample is simulated in terms of a cubic geometry, and losses from the sides and bottom are presented as a function of cube dimensions in terms of optical depth of the excitation wavelength. Monte Carlo results for a homogeneous semi-infinite layer are compared to a simple, fast heuristic model.**
Conclusion: **Both Monte Carlo simulations and the heuristic model clearly detail the volume of tissue interrogated by fluorescence. Since ~ 35–40% of the remitted fluorescence is due to photons originally directed away from the surface, distal layers affect the remitted fluorescence. Fluorescence spectra from small biopsy samples may not produce the correct line shape owing to wavelength dependent losses. Lasers Surg. Med. 21:166–178, 1997.** **© 1997 Wiley-Liss, Inc.**

Key words: Monte Carlo; fluorescence; light propagation; sample size

INTRODUCTION

A rapidly expanding technique for diagnosis of tissue is the measurement of fluorescence [1]. The procedure requires the irradiation of tissue with either a cw or pulsed low level light source at some wavelength λ_x and a measurement of the resulting autofluorescence spectrum. In this report, we examine several factors that affect the measurement and interpretation of fluorescence. This is accomplished through a series of Monte Carlo simulations based upon an excitation wavelength λ_x and emission signal at wavelength λ_m where $\lambda_m \geqslant \lambda_x$. The flexible Monte Carlo technique allows us to vary optical properties such as the wavelength dependent absorption and scattering and to determine the importance of optical boundary conditions and tissue geometry.

The magnitude of fluorescence at λ_m will depend on

(1) the fluence rate distribution of excitation light, $\phi(\mathbf{r},\lambda_x)$ [W/m^2], where $\boldsymbol{r}$ is the position vector x,y,z,

Contract grant sponsor: Albert and Clemmie Caster Foundation; Contract grant sponsor: US Office of Naval Research; Contract grant number: N00014-91-J-1564

*Correspondence to: Dr. A.J. Welch, Department of Electrical and Computer Engineering, University of Texas at Austin, Austin, TX 78712.

Accepted 14 October 1996.

(2) the product of the absorption coefficient and quantum yield of tissue fluorophores, and
(3) the attenuation of the fluorescence light by absorption and scattering in tissue.

Unfortunately, the measured fluorescence spectrum (line shape) emitted from tissue seldom matches the intrinsic line shape of tissue fluorophores, i.e., the spectrum of an optically dilute sample that is not altered by scattering and absorption. The wavelength dependent optical properties of tissue chromophores (such as blood) causes an attenuation of the fluorescence spectrum generated by fluorophores distributed throughout tissue [2].

In addition, scattering modifies the direction of light propagation and ultimately alters the detected fluorescence magnitude and possibly the distribution of escape angles. Monte Carlo simulations provide a straightforward, easy-to-use method for examining these effects. Various optical properties, boundary conditions, and tissue inhomogeneities can be rapidly examined. Most important, excitation and collection geometries can be tested to optimize system performance.

The distribution of excitation light and the filtering effect of tissue at excitation and emission wavelengths can be estimated using a Monte Carlo model that simulates the propagation of photons through tissue. Monte Carlo modeling produces results that are in agreement with solutions based upon transport theory for light propagation in a turbid medium [3]. The governing equation is

$$\frac{dL}{ds}(\mathbf{r},\mathbf{s}) = -\mu_a L(\mathbf{r},\mathbf{s}) - \mu_s L(\mathbf{r},\mathbf{s}) + \int_{4\pi} p(\mathbf{s},\mathbf{s}')L(\mathbf{r},\mathbf{s}')d\omega' \qquad (1)$$

where

L is the radiance [W/(m^2 sr)],
μ_a is the absorption coefficient [1/m],
μ_s is the scattering coefficient [1/m],
p is the phase (single scattering) function [1/sr], and
$d\omega$ is the solid angle in spherical coordinates ($\sin\theta d\theta d\varphi$) [sr]

The radiance $L(\mathbf{r}, \mathbf{s})$ at position ($\mathbf{r} = x,y,z$) in the unit direction **s** is reduced by absorption and scattering and increased by light that is scattered from unit direction **s**′ to unit direction **s.** The probability density function for scattering is governed by the phase function $p(\mathbf{s},\mathbf{s}')$.

The Monte Carlo model provides a basis for simulating photon propagation in a homogeneous medium with random scatterers and absorbers. The light distribution produced by a finite radius, collimated excitation beam is obtained in a two-step process. First, the light distribution for a ray of light is computed. The second step is to convolve the ray response with the function representing the distribution of light on the tissue (irradiance), $E(x,y)$ [W/m^2].

Our fixed weight Monte Carlo computer program injects individual photons into the simulated medium normal to the x,y plane at a specified location (usually at $\mathbf{r} = 0$). The concept of photon movement is analogous to a three-dimensional random walk simulation. Each path length of the random walk corresponds to the distance a photon travels from a scattering event to the next scattering or absorption event. Direction is set by the angle of scattering from the original direction of propagation **s** to the new direction of propagation **s***. The distance between events and the scattering angle are random variables that are a function of the attenuation coefficient $\mu_t = \mu_a + \mu_s$ and phase function, respectively [3].

The distance between events Δs is

$$\Delta s = -\frac{\ell n(\text{Random})}{\mu_t} \qquad (2)$$

where "Random" is a random number in the range [0, 1]. If Henyey-Greenstein scattering is assumed [4], then the angle θ between **s** and **s*** is given by

$$\cos\theta = \frac{1}{2g}\left\{1 + g^2 - \left[\frac{1 - g^2}{1 - g + g(\text{Random})}\right]^2\right\} \quad \text{for } g \neq 0 \qquad (3a)$$

The direction **s*** is specified by selecting an angle φ about **s**

$$\varphi = 2\pi(\text{Random}) \qquad (3b)$$

Random path lengths for a photon are computed until the photon is absorbed or leaves the medium. Then a new photon is inserted. This process continues until the propagation of a specified number N of photons has been accomplished. The fluence rate distribution for a ray of light follows from the absorption pattern of thousands of pho-

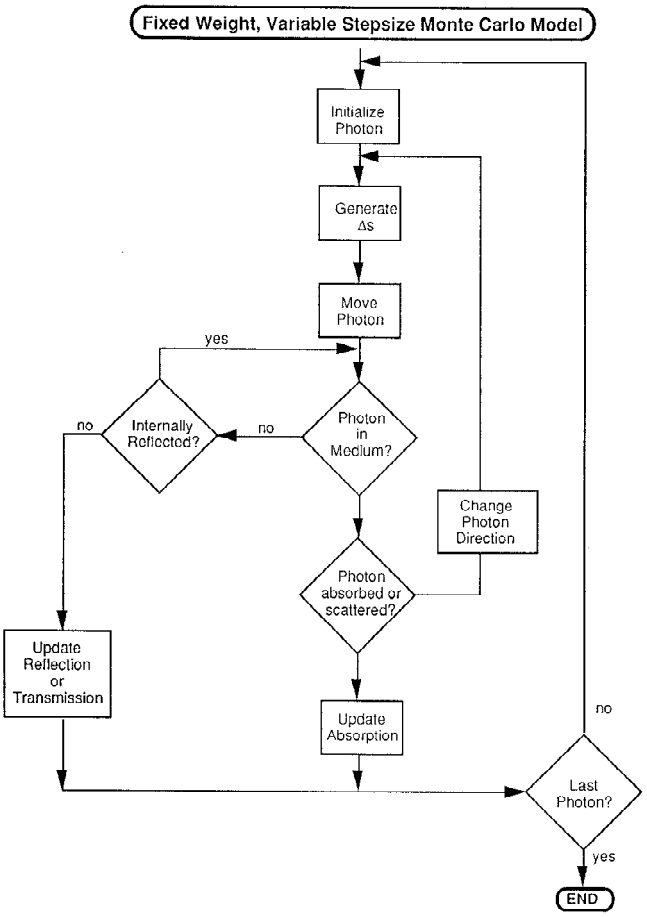

Fig. 1. Flowchart for single photon, variable stepsize Monte Carlo technique.

tons injected into the medium. The fluence rate $\phi_n(\mathbf{r})$ per unit input for any small volume $\Delta V(\mathbf{r})$ is given by

$$\phi_n(\mathbf{r}) = \frac{N_a(\mathbf{r})}{\Delta V(\mathbf{r}) N \mu_a(\mathbf{r})} \tag{4}$$

where $N_a(\mathbf{r})$ is the number of photons absorbed in $\Delta V(\mathbf{r})$, N is the total number of photons in the simulation, and $\mu_a(\mathbf{r})$ is the local absorption coefficient at the wavelength of interest λ. The fraction of irradiance reflected (backscattered) or transmitted is given by the ray response. The Monte Carlo simulation of photon movement is depicted in the flow chart of Figure 1.

MONTE CARLO FLUORESCENCE MODEL

The propagation of the excitation ray is simulated with the fixed weight (single photon) model of Figure 1. The total number of photons

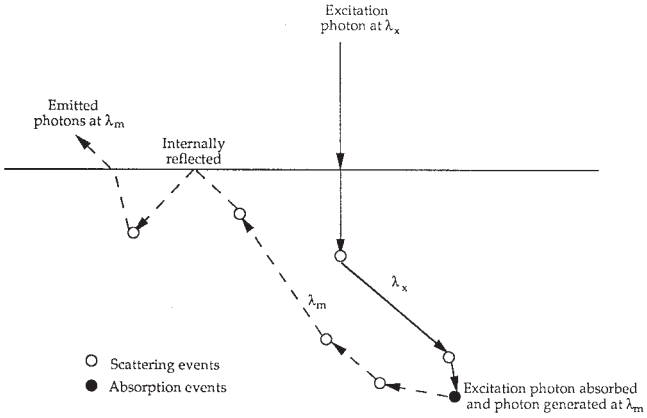

Fig. 2. Random walk nature of Monte Carlo simulation for fluorescence. Solid line represents a path of an excitation photon and the dotted line is a path of emission photon.

remitted from the top surface of the medium yields the diffuse reflectance, R_x. Propagation of the generated photon requires a separate Monte Carlo program to accommodate the optical properties at the emission wavelength, λ_m and to permit "weighting" of the generated photon. A similar simulation has been described by Wu *et al.* [5].

At the point of creation, the photon at the fluorescence wavelength is given a direction $\hat{\mathbf{s}}$ assuming isotropic generation (i.e., all directions are equally likely). From this point, the propagation of the photon is simulated using a weighted photon model [4]. At the end of propagation distance Δs given by equation (2) for $\mu_t(\lambda_m)$, a fraction of the photon is absorbed according to $\mu_a/(\mu_a + \mu_s)$, and the remainder of the photon continues in a random walk through the medium until the weight becomes so small the photon is terminated or the remnant photon crosses a boundary of the simulated tissue.

When a photon crosses a boundary, it is necessary to determine if the photon is reflected or transmitted. Internal reflection is based upon the Fresnel reflection coefficient for unpolarized light. The random walk nature of the simulation is illustrated in the cartoon of Figure 2 and the algorithm for the overall process is depicted in Figure 3. The photons at wavelength λ_m that cross the top surface represent measurable fluorescence.

The weighted photon model for fluorescence reduces computation time for statistically meaningful results. The initial weight of the generated photon can be set to reflect the product of the fluorophore absorption coefficient and the local quantum yield. For homogeneous tissue with a single quantum yield, the initial weight can be set

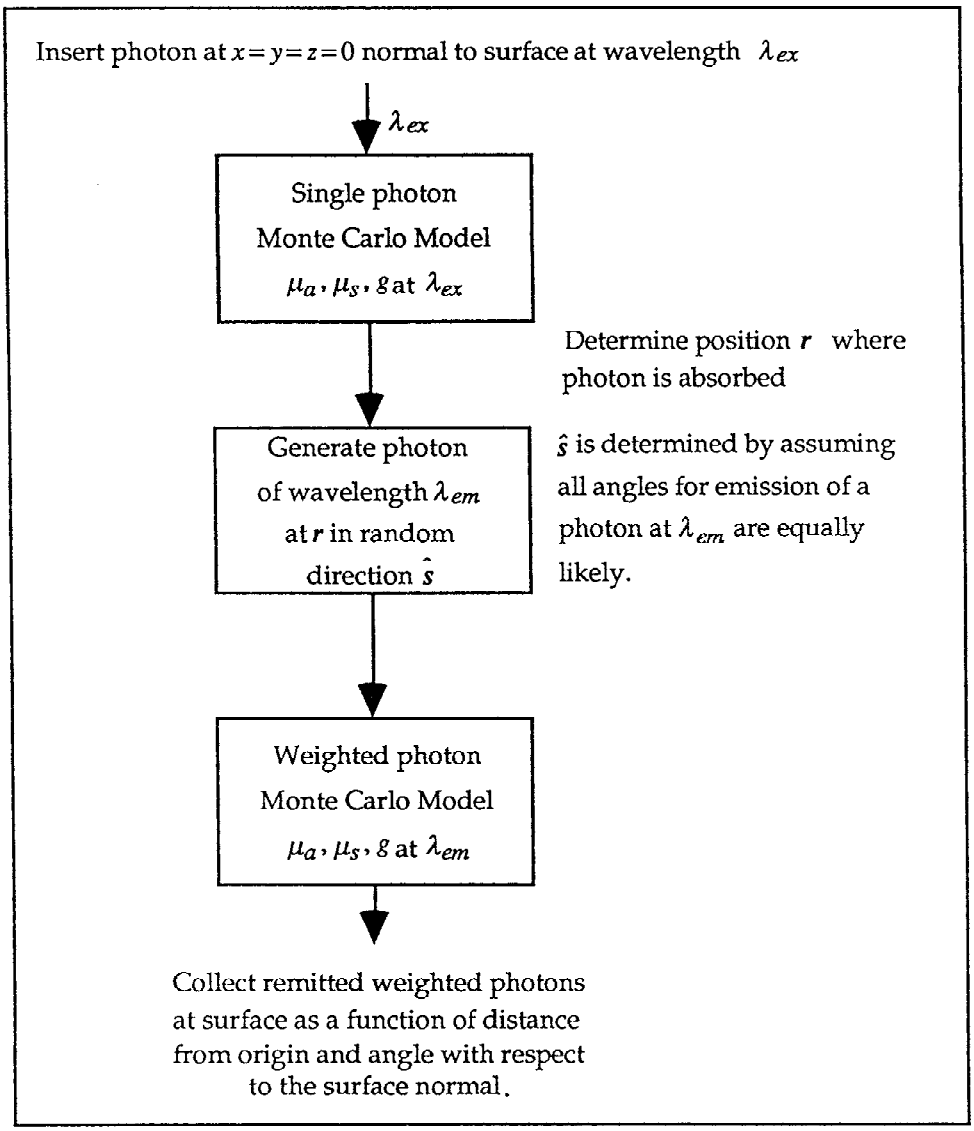

Fig. 3. Block diagram for simulation of fluorescence.

to one; once the simulation is completed, the simulated fluorescence can be multiplied by the product of the fluorophore absorption coefficient and the actual quantum yield to obtain the expected fluorescence.

We compared the results of a weighted photon model for excitation propagation to results from the fixed weight photon model illustrated in Figure 1. The weighted photon model did not seem to improve the accuracy. The weighted photon simulation for modeling the propagation of excitation light was considerably more difficult to write because of the bookkeeping required to track a number of weighted fluorescent photons generated by each weighted excitation photon.

We used Monte Carlo simulations to examine the influence of scattering and the effect of tissue geometry on the measured fluorescence spectrum. These studies were initiated as projects for a graduate class and later expanded for this report. All students that provided results are included as authors. Specifically, we describe photon propagation for a single excitation wavelength (476 nm) and single emission wavelength (600 nm). Although simulations are based upon the optical properties of human aorta, the intent is to examine the general process of fluorescence in a scattering medium.

Initially, we simulated fluorescence in a semi-infinite medium (one and two layers) to de-

TABLE 1. Optical Properties for One and Two Layer Simulation (Uniform Quantum Yield)*

Wavelength	μ_a	μ_s	g	μ_{eff}	δ_{eff}
Intima					
476 nm	7.5 cm^{-1}	240 cm^{-1}	0.85	31.39 cm^{-1}	0.32 mm
600 nm	3.0 cm^{-1}	170 cm^{-1}	0.84	16.5 cm^{-1}	0.61 mm
Media					
476 nm	6.5 cm^{-1}	412 cm^{-1}	0.89	31.39 cm^{-1}	0.32 mm
600 nm	2.0 cm^{-1}	323 cm^{-1}	0.89	16.5 cm^{-1}	0.61 mm

*Intima optical thickness for single layer simulation and 0.3 mm for two layer simulation.

termine the regions of tissue that contribute to the remitted fluorescence. Information required to calculate the signal collected by various detectors was obtained from distributions of photon exit angle and exit distance relative to a narrow excitation beam. To understand where fluorescence is generated that produces a measurable signal at the surface, we determined the frequency of occurrence of fluorescence photons as a function of depth that eventually escaped from the tissue. These simulations provided comparisons for index matched and mismatched surface boundary conditions and difference between a homogeneous medium and a medium with two layers.

Since preliminary simulations suggested that a significant percent of fluorescent photons are initially directed away from the surface, we determined if distal layers affected the fluorescence signal. A series of multiple layer simulations were performed. Also, the multiple layer simulations provided an opportunity to examine the effect of having different quantum yields for each layer. We tested the hypothesis that fluorescence was correlated to the thickness of a necrotic layer of fat in a heterogeneous vessel layer.

Next, the question of the effect of the physical size of a sample upon fluorescence was examined. We simulated the amount of light that escapes from the bottom and sides of small volumes in the shape of cubes. The results provided an estimate on the minimum size biopsy that is suitable for fluorescence testing.

Last, an approximate escape function [6] was compared to Monte Carlo simulations for the depth-resolved fluorescence remitted by a homogeneous semi-infinite slab with uniform illumination. This rapidly computed approximation provided results in close agreement to the computationally intensive Monte Carlo simulation. The fluorescence remittance due to all fluorophores located within depths 0 to z, $R_m(z)$, normalized to the remittance due to all fluorophores, R_m, may be written as

$$\frac{R_m(z)}{R_m} = \frac{\int_0^z \phi(z';\lambda_x)G(z';\lambda_m)dz'}{\int_0^\infty \phi(z';\lambda_x)G(z';\lambda_m)dz'} \tag{5}$$

where ϕ is the one-dimensional distribution of excitation light [W/m] and G is the fraction of emission escape due to fluorophores at depth z. The product ϕG, therefore, represents the probability that an emission fluorescence photon generated at z will escape to the top surface of the slab, weighted by the number of emission photons generated at z (which is proportional to the number of excitation photons present at z). The ratio $R_m(z)/R_m$ represents the fraction of total remittance due to fluorophores located within the depth z; it may therefore be used to study the probing depth of a surface delivery and collection fluorescence measurement. Analytic expressions for ϕ and G based upon Monte Carlo simulations can be used to investigate $R_m(z)/R_m$.

Using these expressions [6] for the distribution of excitation light, $\phi(z';\lambda_x) = C_1 \exp(-k_1 z'/\delta_{eff}(\lambda_x)) - C_2 \exp(-k_2 z'/\delta_{eff}(\lambda_x))$, and escape function, $G(z';\lambda_m) = C_3 \exp(-k_3 z'/\delta_{eff}(\lambda_m))$, Eq. 5 may be rewritten as

$$\frac{R_m(z)}{R_m} = 1 - \frac{A \exp(-k_1 z/\delta_{eff}(\lambda_x) - k_3 z/\delta_{eff}(\lambda_m)) - B \exp(-k_2 z/\delta_{eff}(\lambda_x) - k_3 z/\delta_{eff}(\lambda_m))}{A - B} \tag{6}$$

where $A = C_1C_3/(k_1/\delta_{eff}(\lambda_x) + k_3/\delta_{eff}(\lambda_m))$ and $B = C_2C_3/(k_2/\delta_{eff}(\lambda_x) + k_3/\delta_{eff}(\lambda_m))$. The parameters C_1, C_2, k_1, and k_2 are functions of the diffuse reflectance at the excitation wavelength, whereas C_3

and k_3 are functions of diffuse reflectance at the emission wavelength (see Table 1 in reference [6] for exact relationships). The optical properties $\delta_{eff}(\lambda_x)$ and $\delta_{eff}(\lambda_m)$ are the effective penetration depths of light at the excitation and emission wavelengths, respectively, as defined by diffusion theory:

$$\delta_{eff} = \frac{1}{\sqrt{3\mu_a(\mu_a + \mu_s(1-g))}} = \frac{1}{\mu_{eff}} \qquad (7)$$

The quantity $R_m(z)/R_m$ was investigated using Eq. 6 for a range of optical properties typical of tissue for visible wavelengths, as described in the Material and Methods section.

MATERIALS AND METHODS

Monte Carlo simulations incorporated the Henyey-Greenstein phase function to determine photon direction. Propagation at boundaries was based on the Fresnel reflection equation for unpolarized light. Optical properties used in these simulations are based upon reported values for normal and atheromatous human aorta. One and two layer, multiple layer, and finite tissue sample simulations represented light distributions for a ray (spot size→0) of photons inserted at $x,y = 0$. The data generated for the approximate escape function represents the response to a uniform irradiance.

One and Two Layer Simulations (uniform quantum yield)

The single layer simulations for matched and mismatched boundary conditions assumed a semi-infinite layer, and used the optical properties of the intima (Table 1) at the excitation and emission wavelengths. The two layer geometry had matched boundary conditions at the surface. The front layer represented a 0.3-mm-thick intima layer and the second infinitely thick media (see Table 1 for optical properties). For mismatched boundary conditions, the index of refractions were $n_{\text{air}} = 1$ and $n_{\text{tissue}} = 1.4$. Optical properties for the layers of aorta at the excitation (476 nm) and emission (600 nm) wavelengths were estimated from the data of Keijzer et al. [7], Çilesiz et al. [8], and Torres et al. [9] (see Table 1). Tissue layers are assumed to have the same index of refraction.

The simulations provided total reflectance, specular, and diffuse (backscattered light) reflectance of the excitation beam R_x. Fluorescence was described in terms of the total remitted fluorescence R_m. The origin and pattern of the fluorescence was characterized by determining

(1) depth of photogeneration for remitted fluorescence,
(2) initial direction of remitted photon,
(3) fluorescence pattern as a function of radial distance from the excitation ray, and
(4) angular distribution of remitted fluorescence.

The excitation ray was normal to the slab in all simulations.

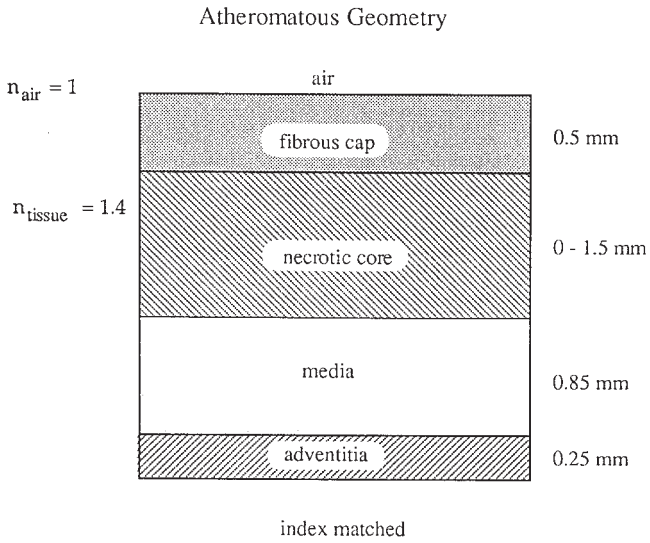

Fig. 4. Layered geometry for Monte Carlo simulation of atheromatous human aorta.

Multiple Layer Simulations (nonuniform quantum yield)

A multiple layered semi-infinite slab, as illustrated in Figure 4, provided a geometry for investigating the effect of nonuniform quantum yields. This slab represented the assumed geometry for atheromatous human aorta in that a fatty necrotic core (NC) is covered by a fibrous cap. Actual lesions do not have a regular shape as suggested in Figure 4. Nevertheless, as a lesion grows in size, it reduces the lumen of the vessel.

For this simulation it was necessary to assume parallel layers. Although the bulk sample was heterogeneous, each layer was homogeneous with the optical properties and intrinsic fluorescence coefficients given in Tables 1 and 2. Thickness and index of refraction of each layer are given in Figure 4.

TABLE 2. Optical Properties for Atheromatous Human Aorta (nonuniform quantum yield)

	λ_x = 476 nm			λ_m = 600 nm				
Layer	μ_a (cm^{-1})	μ_s (cm^{-1})	g	μ_a (cm^{-1})	μ_s (cm^{-1})	g	Thickness (mm)	Fluorescence coefficient ($\cdot 10^{-5}$ cm^{-1})
Fibrous cap	13	412	0.89	4.0	331	0.89	0.5	2.8
Necrotic core	6.5	412	0.89	2.0	331	0.89	0–1.5	25.0
Intima	7.5	240	0.85	3.0	170	0.84	0.3	4.5
Media	6.5	412	0.89	2.0	323	0.89	0.85	8.2
Adventitia	15	270	0.75	5.0	215	0.76	0.25	5.5

Optical properties and quantum yields for the fibrous cap and necrotic core were based on discussions with Richards-Kortum [10]. These properties were estimated from fluorescence photomicrographs of atherosclerotic aorta and are somewhat arbitrary since neither has been measured for these plaque layers. Nevertheless, we assumed that these optical properties were related to those of the media. The absorption coefficient of the fibrous cap was set at two times that of the media, and the absorption coefficient of the necrotic core was given the same value as the media. Scattering coefficients of the plaque layers were equal to those of the media. The fluorescence quantum yield of the fibrous cap was set at one-third of the media quantum yield and quantum yield of the necrotic core was three times the value in the media. The thickness of the necrotic core was varied from 0 mm to 1.5 mm to determine if the remitted fluorescence provided information on thickness of the necrotic core. Each simulation consisted of 10^6 excitation photons.

Finite Tissue Sample

The grid geometry and code of the Monte Carlo program were modified to include side boundary conditions for a tissue-air interface. Internal reflections of the side boundaries were considered in addition to those at the top and bottom surfaces to represent the geometry of a biopsy sample.

Once again, the optical properties of aorta intima at 476 nm and 600 nm (Table 1) were used in this simulation. The index of refraction of tissue was 1.4 and that of air 1.0. The sample was assumed to be a small cube with all sides of equal length. Six simulations were computed for a cube whose linear dimension ranged from 0.4 to 10 mm (see Table 4). Each simulation contained 10^5 photons.

Approximate Escape Function

The probing depth of a fluorescence measurement, z_{probe}, was defined as the depth above which 90% of the remitted fluorescence originates. This probing depth was determined for a range of tissue optical properties using the relationship in Eq. 6 between $R_m(z)/R_m$ and the diffuse reflectance and effective penetration depth at the excitation and emission wavelengths. The quantity $R_m(z)/R_m$ was plotted as a function of dimensionless depth, $(1/\delta_{eff}(\lambda_x) + 1/\delta_{eff}(\lambda_m))z$, for diffuse reflectances ranging independently from 0.05 to 0.4 at λ_x = 476 nm and λ_m = 600 nm, and for effective penetration depths at the two wavelengths ranging independently from 0.01 to 1 cm. The probing depth was calculated for $R_m(z_{probe})/R_m = 0.9$.

RESULTS

One and Two Layer Simulations (uniform quantum yield)

Based on the optical properties of Table 1 and using equation (7), the effective penetration depths at excitation and at the emission wavelengths for the intima and media are shown in Table 1. The fraction of reflected light at the excitation wavelength R_x and the fraction of fluorescence escaping at the surface R_m are presented in Table 3 for a single semi-infinite geometry and for a two layered geometry.

A plot of total fraction of fluorescent photons remitted that originate at depth z for the three conditions of Table 3 is given in Figure 5. These values are normalized with respect to the total remitted fluorescence for each condition. As a result, each curve represents the percent of remitted light originating at depth $z \pm \frac{1}{2}\Delta z$. The effect of internal reflectance given in Table 3 is not seen in these curves because of the normalization. The remitted light of Figure 5 contains a number of photons that had an initial downward direction. At any depth, ~37% of the remitted photons were initially directed away from the top surface. Also, the simulations confirm the assumption that the angular distribution of light remitted from the

TABLE 3. Total Remitted Light at Excitation and Emission Wavelengths for Three Conditions*

Tissue geometry and boundary condition	R_x	R_m
Intima, mismatched	0.186	0.236
Intima, matched	0.275	0.314
Intima/media, matched	0.289	0.342

*In each simulation, absorbed photons were converted to emission photons with 100% efficiency.

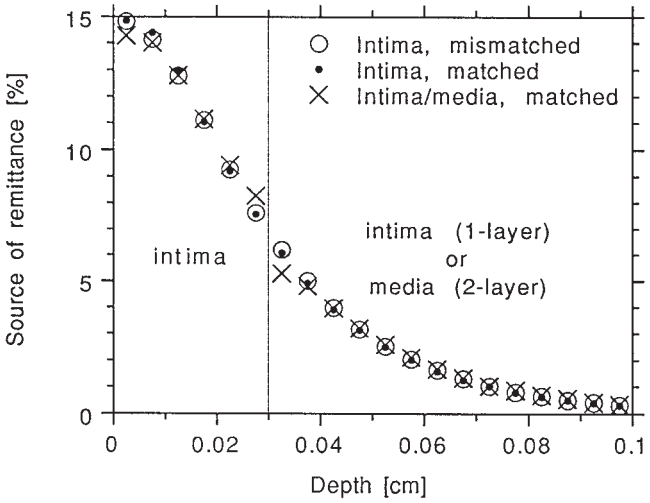

Fig. 5. Remitted fluorescence as a function of depth of fluorescence generation.

surface is Lambertian (results not shown). Simulation results for exit position are given in Figure 6. Once again, the data is normalized to represent remitted photons at radius $r \pm \frac{1}{2}\Delta r$. Table 3 and Figures 5 and 6 illustrate the differences in matched and mismatched boundary conditions.

Multiple Layer Simulations (nonuniform quantum yield)

The source of fluorescence for the multiple layered aorta structure of Figure 4 is illustrated in Figure 7 for normal (intima, media, adventitia) and diseased (fibrous cap, necrotic core, media, adventitia) aorta. The overall effect of fluorescence as a function of necrotic core thickness is presented in Figure 8. The fibrous cap reduces the total fluorescence by a factor of approximately 2.5. Increasing the thickness of the necrotic core slightly increases total fluorescence.

Finite Tissue Sample

The fraction of fluorescence photons remitted from the top, bottom, and sides of a small tissue sample (cube) with a ray of excitation light

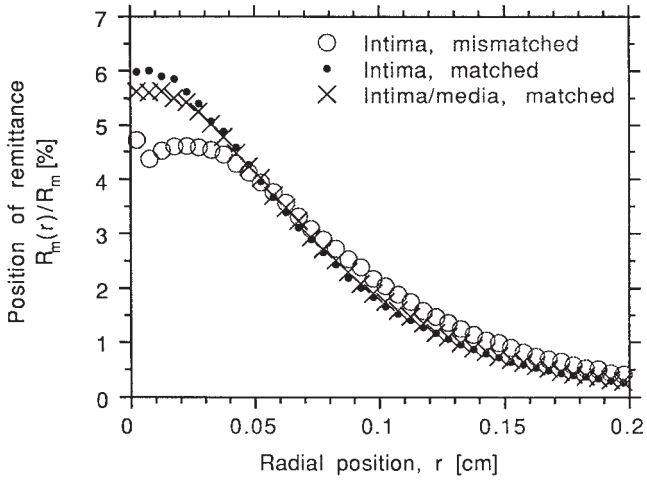

Fig. 6. Remitted fluorescence as a function of radial escape position.

are presented in Table 4. The physical dimensions of 0.4 to 10.1 mm represented optical depths ($\delta = 1/\mu_t$) of 10–250 for the optical properties of intima at the excitation wavelength of 476 nm as listed in Table 1. Since the simulations employed a unit quantum yield, the total number of photons generated by fluorescence was equal to the number of absorbed excitation photons. The fraction of excitation photons absorbed or remitted from the top surface are included in Table 4. Figure 9 shows the percent of absorbed photons and the percent fluorescence photons reabsorbed or remitted from the top, sides, and bottom of the cube as a function of cube dimensions. For the optical properties used in this simulation, the cube must have dimensions >5 mm for fluorescence measurements to be independent of tissue sample dimensions.

Approximate Escape Function

The depth dependence of the ratio $R_m(z)/R_m$ was found to be exponential with the dimensionless parameter $(1/\delta_{eff}(\lambda_x) + 1/\delta_{eff}(\lambda_m))z$, and approximately independent of the diffuse reflectance at the excitation and emission wavelengths. It was found that the expression in Eq. 6 accurately represents $R_m(z)/R_m$ for tissue with absorption-dominant (diffuse reflectance <0.05) and scattering-dominant (diffuse reflectance >0.2) optical properties. For example, in Figure 10, where scattering dominates absorption, the fraction of remitted fluorescence due to fluorophores above depth z calculated using Eq. 6 is compared to Monte Carlo simulation result for a semi-infinite slab of intima with optical properties listed in Table 1. The probing depth of a surface fluores-

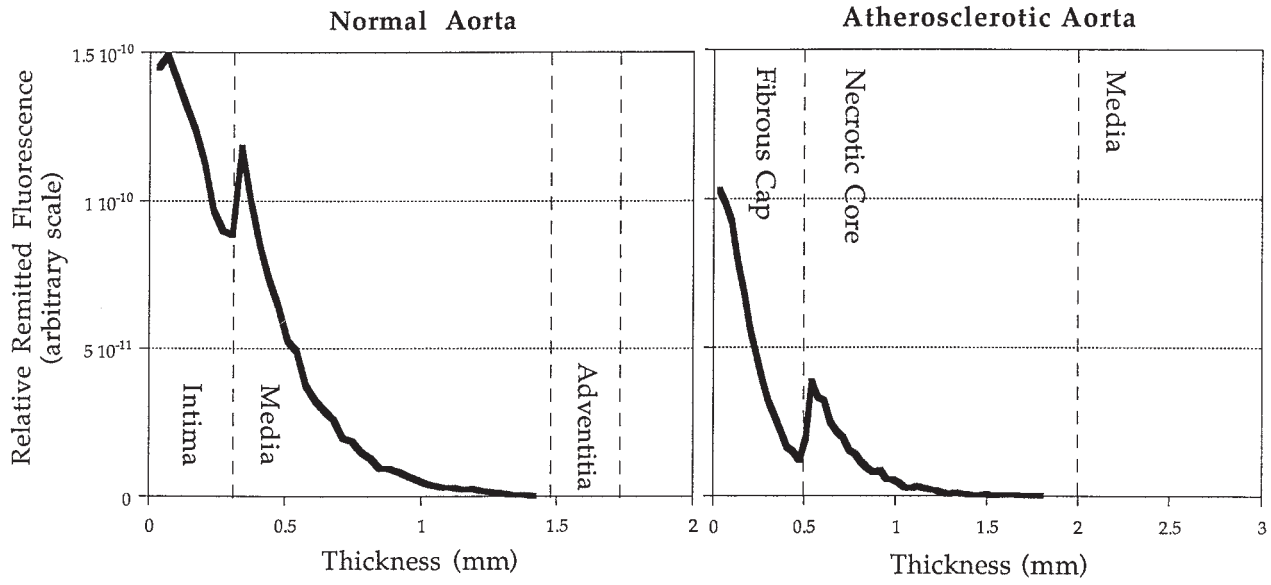

Fig. 7. Remitted fluorescence as a function of depth of fluorescence generation. Tissue geometries simulated represent normal aorta and atherosclerotic aorta with a fibrous cap and 1.5 mm necrotic core (optical properties given in Table 2).

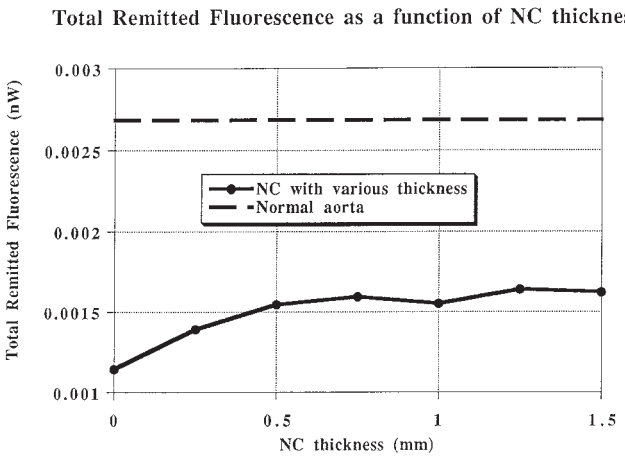

Fig. 8. Total remitted fluorescence as a function of necrotic core thickness. Remitted fluorescence for normal aorta is plotted for comparison.

cence measurement ranged from $2.4/(1/\delta_{eff}(\lambda_x) + 1/\delta_{eff}(\lambda_m))$ to $3.2/(1/\delta_{eff}(\lambda_x) + 1/\delta_{eff}(\lambda_m))$ for the wide range of optical properties investigated. The mean value $z_{probe} = 2.7/(1/\delta_{eff}(\lambda_x) + 1/\delta_{eff}(\lambda_m))$ is accurate to within 20% of the true value, for diffuse reflectance between 0.05 and 0.4 at the excitation and emission wavelengths.

DISCUSSION

One and Two Layer Simulations (uniform quantum yield)

The first group of simulations may be used to investigate the effects of boundary conditions and tissue geometry for the one-dimensional slab case. In Table 3, it is evident that an index mismatched boundary reduces the total fraction of excitation and emission photons that are remitted from the medium surface. An index mismatch produces internal reflectance at the surface boundary, allowing many of these reflected photons to be absorbed. However, when the source of fluorescence (Fig. 5) is normalized with respect to total fluorescence, then the curves are almost identical. That is, index matching does not affect the fluorescence line shape nor the contribution of each depth in the remitted fluorescence. It does affect the signal to noise ratio of the measurement. The two layer intima-media geometry increases the fraction of remitted photons with respect to the single layer geometry because the second layer has a lower absorption coefficient and higher scattering than the top layer. Photons traveling through the second layer have a smaller probability of absorption and a therefore larger probability of remission. An opposite effect would be observed for a bottom layer with lower scattering and higher absorption than the top layer.

If the second layer is optically close to the surface (less than two optical depths away), optical properties of a second layer will change the source pattern of remittance (Fig. 5) for two reasons. First, higher scattering and lower absorption of the bottom layer will allow more fluorescence generated in the top layer to diffuse to the surface. The decay of the fluorescence source gen-

TABLE 4. Distribution of Remitted Light from a Cube with the Optical Properties of Intima Listed in Table 1*

Cube dimension		Excitation [% Delivered]		Fluorescence [% generated]		
[mm]	[OD(λ_x)]	Remitted top	Absorbed	Remitted top	Remitted sides	Remitted bottom
0.40	10	8.4	32.5	17.1	58.8	13.3
1.01	25	13.7	61.2	20.3	45.3	7.2
2.02	50	16.3	76.8	25.2	24.6	2.0
3.03	75	16.5	80.1	27.6	11.8	0.5
5.05	125	16.7	80.7	29.3	2.3	0.0
10.1	250	16.8	80.7	29.5	0.0	0.0

*In the simulations, excitation photons were converted to emission photons with 100% efficiency. Optical depth is ($1/\mu_t$).

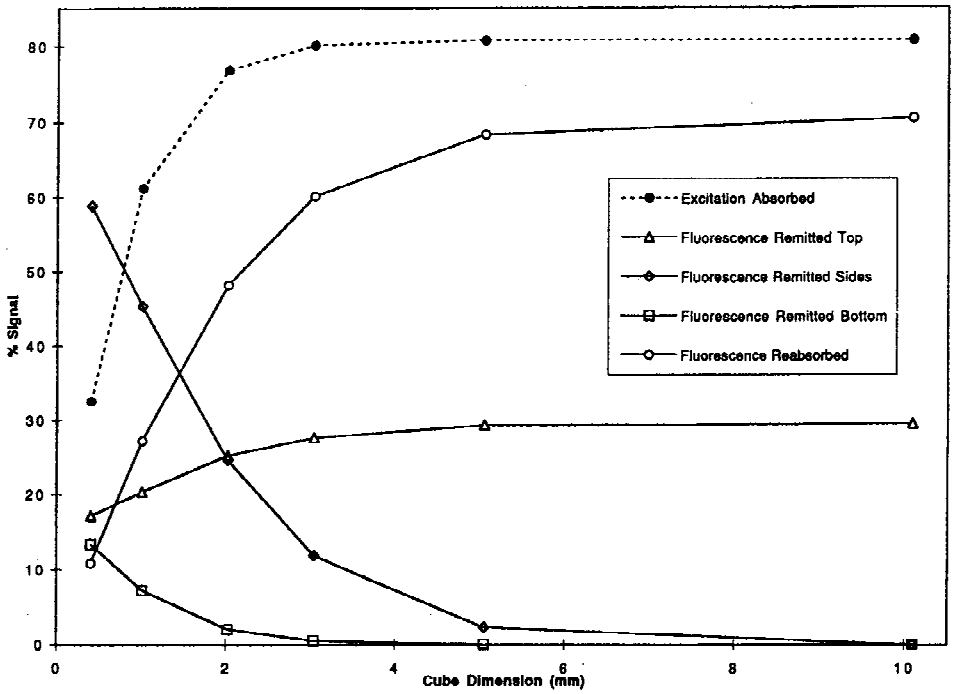

Fig. 9. Percent of absorbed photons and the percent of fluorescence photons reabsorbed or remitted from the top, sides and bottom of a cube of tissue as a function of cube dimensions.

eration pattern in the intimal layer will be slightly more gradual in the intima/media tissue than the intima tissue. Second, there is a discontinuity in the source pattern at the intima/media boundary because of the discontinuity in absorption coefficient, which controls the local rate of fluorescence photon generation.

Neither boundary conditions nor tissue optical properties affect the angular pattern of remission. Fluorescence escape from turbid media are approximately Lambertian, i.e., the remitted power per unit solid angle varies with the cosine of exit angle. Boundary conditions do affect the spatial pattern of remittance at the tissue surface (Fig. 6). A mismatched boundary produces a wider pattern of fluorescence escape in part because internally reflected fluorescence photons diffuse farther from the optical axis before escaping. Thus placement of a small detector (diameter $\leqslant$100 μm) is more critical for index matched detection than nonindex matched; however, there is a significant decrease in detected fluorescence for a detector not index matched with the surface.

Multiple Layer Simulations (nonuniform quantum yield)

In the simulations modeling atheromatous aorta, there was a decrease in remitted fluorescence due to the fibrous plaque and necrotic core layers (Figure 7). The two atherosclerotic layers had lower intrinsic fluorescence coefficients than the intima and media (see Table 2); therefore, fewer emission photons were generated in these layers than in the normal aorta tissues. The

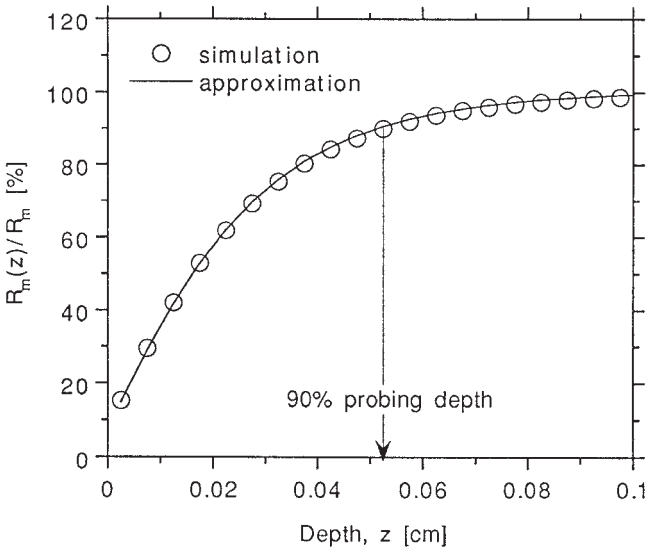

Fig. 10. The percentage of remitted fluorescence due to fluorophores above depth z, $R_m(z)/R_m$, calculated using the approximation in Eq. 6 is compared to the Monte Carlo simulation result. For both the approximation and simulation, a semi-infinite slab of intima with optical properties listed in Table 1 was modeled. The depth above which 90% of the total remitted fluorescence originates is marked with the arrow.

rather large absorption coefficient of the fibrous cap reduced the amount of excitation light reaching the media even when the necrotic core was optically thin. This significantly reduced the contribution of remitted fluorescence due to photogeneration in the normal aorta layers (Fig. 7). The reduction in excitation light also affected the detection of fluorescence from the necrotic core. Even though the fluorescence coefficient of the necrotic core was almost ten times larger than the fluorescence coefficient of the fibrous cap (see Table 2), increasing the thickness of the necrotic core beyond 0.5 mm did not significantly increase the total remitted fluorescence (see Fig. 8). For this single set of measurements, total fluorescence is not a very good indicator of necrotic core thickness. This agrees well with experimental results, which have failed to show a correlation between necrotic core thickness and measured fluorescence over large ranges in necrotic core thickness.

Predictive information requires measurements at several emission wavelengths. Considerable progress has been reported by Richards-Kortum [11] and Deckelbaum et al. [12] in the recognition of atheromatous and normal aorta. Typically the most important information is the ratio of fluorescence measurements at selected wavelengths and processing of the raw fluorescence measurement to account for the filtering effect of the tissue [11].

Finite Tissue Sample

In vitro fluorescence measurements of tissue biopsy samples have been used to determine the feasibility of diagnostic spectroscopy [13] and later to form algorithms for in vivo detection or diagnosis [14]. As seen in Table 4 and Figure 9, the fluorescence reaching the front surface of a tissue cube is a strong function of the cube volume relative to the tissue optical properties. A cube with dimensions greater than approximately 125 optical depths at the excitation wavelength approaches a semi-infinite tissue geometry for the optical properties simulated, i.e., fluorescence escapes solely from the top surface. Figure 9 shows that for optical properties of intima, a 1.0 cm cube meets these criteria. However, such a large specimen is not practical.

The percent of excitation light absorbed and the percent of fluorescence reabsorbed and remitted from the sides and bottom change rapidly as the cube dimension increases from 0.4 mm (smallest dimension tested) to 4.0 mm. Figure 9 suggests when only small biopsies are available for in vitro studies that the biopsy dimension should be at least 75–100 optical depths (excitation wavelength), which is 3.0–4.0 mm for arterial tissue for results to most closely resemble fluorescence spectra expected from intact tissue. Below this limit, both the amount of signal remitted will be a strong function of tissue size. Most important, the optical depth of the cube relative to emission wavelength will vary over the emission spectrum, causing the fluorescence line shape to be a function of tissue size.

For most soft tissue, the scattering coefficient will decrease with wavelength and the absorption coefficient between 500 nm and 650 nm will be dependent upon the blood concentration in the tissue [8].

Approximate Escape Function

It may be important to estimate the depths probed by a fluorescence measurement. The approximate escape function provides a simple method to estimate this probing depth. From the approximate expression $z_{probe} = 2.7/(1/\delta_{eff}(\lambda_x) + 1/\delta_{eff}(\lambda_m))$, one can see that the effective probing depth of a typical fluorescence measurement is proportional to $\delta_{eff}(\lambda_x)$ if $\delta_{eff}(\lambda_x) \ll \delta_{eff}(\lambda_m)$, $\delta_{eff}(\lambda_m)$ if $\delta_{eff}(\lambda_x) \gg \delta_{eff}(\lambda_m)$ and $\delta_{eff}(\lambda_x)/2$ if $\delta_{eff}(\lambda_x) \approx \delta_{eff}(\lambda_m)$. As seen in Figure 10, the pattern of re-

TABLE 5. Potential Inaccuracies of Fluorescence Measurements and Their Interpretation

Sample size requirements:	• Sampling depth depends on optical properties at the excitation and emission wavelength. 90% of the fluorescence originates from depths above $z_{90\%} = 2.7/(1/\delta_{eff}(\lambda_x) - 1/\delta_{eff}(\lambda_m))$. • Tissue below $z_{90\%}$ can affect fluorescence, since 30–40% of fluorescence photons remitted from the tissue surface are initially directed downward. • The intensity and spectral shape of fluorescence and reflectance remitted from the surface of a small biopsy is a strong function of sample size when the biopsy dimensions are less than 75–100 optical depths at the excitation wavelength.
Sample conditions:	• Index matching at the front surface of the sample produces approximately a 50% increase in remitted reflectance and fluorescence relative to mismatched conditions. This boundary condition does not affect spectral shape or sampling depth, however.
Emission pattern:	• Although fluorescence is generated isotropically within tissue, the angular distribution of remitted fluorescence is Lambertian for all optical properties and boundary conditions. Mismatched boundary conditions produce more radial spreading of the remitted reflectance and fluorescence.

mitted fluorescence generation approximated by an approximate equation closely matches the Monte Carlo simulation result. Using the simulation data, the 90% probing depth for a semi-infinite slab of intima index mismatched with air is $z_{probe} = 520$ μm. For human intima, $\delta_{eff}(\lambda_x) = 320$ μm for 476 nm excitation, and $\delta_{eff}(\lambda_m) = 610$ μm for 600 nm emission; therefore the estimated probing depth of the fluorescence measurement is $z_{probe} \approx 500$ μm.

CONCLUSION

Monte Carlo simulations provide a realistic method for interpreting the effects of geometry upon remitted fluorescence. Since a significant percent (35–40) of the remitted fluorescence in this simulation is initially directed away from the surface, distal layers may influence the remitted fluorescence. More striking is the effect of the size of the tissue sample upon the remitted fluorescence. When the optic depth ($1/\mu_t$) of the excitation light is <50 times the depth of a cubic sample, a majority of the remitted fluorescence escapes from the sides and bottom of the sample. For a specified physical size, the optical size varies as a function of wavelength. That is, for a given excitation wavelength the cube has a different optical size for each emission wavelength. The exact amount will be dependent upon emission wavelength optical properties. Since scattering decreases with wavelength, it is reasonable to expect for an emission wavelength the optical size as a number of optical depths will be smaller than defined by the excitation wavelength. The optical depth ($1/\mu_t$) wavelength will increase with wavelength. Thus any measurement of line shape will be corrupted by the wavelength dependent optical size of the tissue sample relative to the physical size. In general, potential inaccuracies of fluorescence measurements and their interpretation are summarized in Table 5.

When geometry is not a problem and effective optical depths can be estimated, the heuristic algorithm for fluorescence provides excellent results. This algorithm approximates Monte Carlo results over a wide range of optical properties.

Finally, excellent Monte Carlo codes are not difficult to write, and the results that are generated provide insight into light propagation and provide a guide for both in vitro and in vivo experiments. An excellent place to start is to order the well-documented program supplied by Drs. Steve Jacques and Lihong Wang. This may be obtained by contacting Steve Jacques, PhD, Oregon Medical Laser Center, Providence St. Vincent Medical Center, 9205 S. Barnes Rd., Portland, OR 97225; sjacques@ee.ogi.edu

ACKNOWLEDGMENTS

A.J.W. is Marion E. Forsman Centennial Professor of Engineering. This work was supported in part by the Albert and Clemmie Caster Foundation and in part by the US Office of Naval Research under grant N00014-91-J-1564.

REFERENCES

1. Svanberg S. Diagnostic system based on simultaneous multispectral fluorescence imaging, Appl Opt 1994; 33: 8022–8030.
2. Richards-Kortum R, Fluorescence spectroscopy of turbid media. In: AJ Welch, MJC van Gemert, eds. "Optical-Thermal Response of Laser-Irradiated Tissue." New York: Plenum Press, 1995.

3. Keijzer M, Jacques SL, Prahl SA, Welch AJ. Light distributions in artery tissue: Monte Carlo simulations for finite-diameter laser beams. Lasers Surg Med 1989; 9: 148–154.
4. Jacques SL, Wang L. Monte Carlo modeling of light transport in tissue. In: AJ Welch, MJC van Gemert, eds, "Optical-Thermal Response of Laser-Irradiated Tissue. New York: Plenum Press, 1995.
5. Wu J, Feld MS, Rava RP. Analytic model for extracting intrinsic fluorescence in turbid media. Appl Opt 1993; 32:3585–3595.
6. Gardner CM, Jacques SL, Welch AJ. Light transport in tissue: accurate expressions for one-dimensional fluence rate and escape function based upon Monte Carlo simulation. Lasers Surg Med 1996; 18:129–138.
7. Keijzer M, Richards-Kortum R, Jacques S, Feld M. Fluorescence spectroscopy of turbid media: autofluorescence of the human aorta. Appl Opt 1989; 28:4286–4292.
8. Çilesiz IF, Welch AJ. Light dosimetry: effects of dehydration and thermal damage on the optical properties of the human aorta. Appl Opt 1993; 32:477–487.
9. Torres JH, Welch AJ, Motamedi M. Tissue optical property measurements: overestimation of absorption coefficient with spectrophotometric techniques. Lasers Surg Med 1994; 14:249–257.
10. Richards-Kortum R (pers. comm.)
11. Richards-Kortum RR, Rava R, Fitzmaurice M, Tong L, Ratliff NB, Kramer JR, Feld MS. A one-layer model of laser induced fluorescence for diagnosis of disease in human tissue: Applications to atherosclerosis. IEEE Trans Biomed Eng 1989; 36:1222–1232.
12. Deckelbaum LI, Lam JK, Cabin HS, Clubb KS, Long MB. Discrimination of normal and atherosclerotic aorta by laser-induced fluorescence. Lasers Surg Med 1987; 7:330–335.
13. Mahadevan A, Mitchell MF, Silva E, Thomsen S, Richards-Kortum R. Study of fluorescence properties of normal and neoplastic human cervical tissue. Lasers Surg Med 1993; 13:647–655.
14. Schomacker KT, Frisoli JK, Compton CC, Flotte TJ, Richter JM, Deutsch TF, Nishioka NS. Ultraviolet laser induced fluorescence of colonic polyps. Gastroenterology. 1992; 102:1155–1160.